

## Supplementary information

for

### Tracing driving forces responsible for the remarkable infectivity of 2019-nCoV: 1. receptor binding domain in its bound and unbound states

Ziyi Liu<sup>1,2</sup>, Miaoren Xia<sup>2</sup>, Zhifang Chai<sup>2,3</sup>, Dongqi Wang<sup>1,2,\*</sup>

<sup>1</sup> State Key Laboratory of Fine Chemicals, Liaoning Key Laboratory for Catalytic Conversion of Carbon Resources, School of Chemical Engineering, Dalian University of Technology, Dalian 116024, China

<sup>2</sup> Multidisciplinary Initiative Center, Institute of High Energy Physics, Chinese Academy of Sciences, Beijing 100049, China

<sup>3</sup> State Key Laboratory of Radiation Medicine and Protection, and School of Radiation Medicine and Interdisciplinary Sciences (RAD-X), Soochow University, Suzhou 215123, China

E-mail: wangdq@dlut.edu.cn

#### 1. The compositions of the simulated systems

**Table S1.** The compositions of the simulated systems for both 2019-nCoV and SARS-CoV systems.

| Label     | Solute   | N <sub>wat</sub> | Box size (nm) | Production time (ns) |                     |     |
|-----------|----------|------------------|---------------|----------------------|---------------------|-----|
|           |          |                  |               | Plain simulation     | Simulated annealing |     |
| 2019-nCoV | RBD/ACE2 | RBD+ACE2         | 48800         | 9.9×10.8×14.9        | 100                 | -   |
|           | RBD      | RBD              | 18800         | 7.6×8.6×9.1          | 100                 | 100 |
|           | ACE2     | ACE2             | 34476         | 9.9×10.6×10.8        | 100                 | -   |
| SARS-CoV  | RBD/ACE2 | RBD+ACE2         | 48800         | 9.9×10.8×14.9        | 100                 | -   |
|           | RBD      | RBD              | 18800         | 7.6×8.6×9.1          | 100                 | 100 |
|           | ACE2     | ACE2             | 34476         | 9.9×10.6×10.8        | 100                 | -   |

#### 2. The energy decomposition in the recognition of ACE2 to RBD

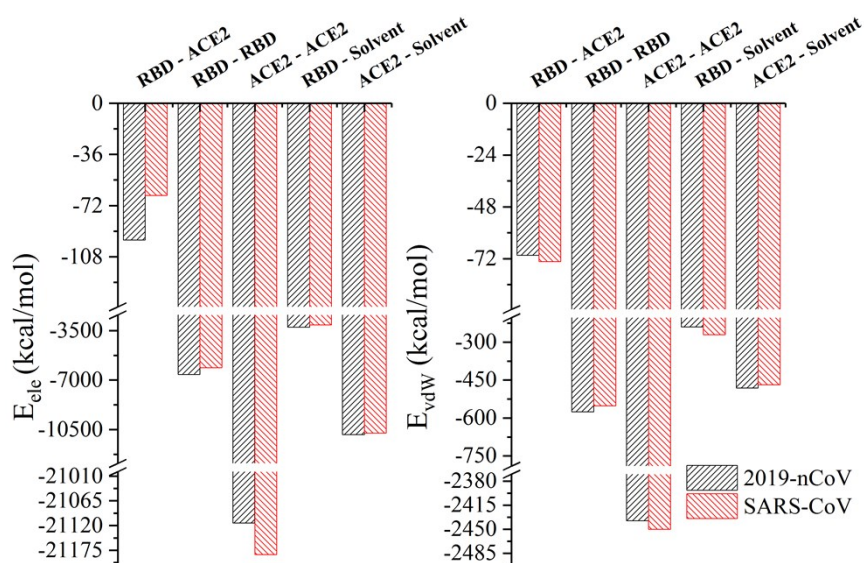


**Figure S1.** Decomposition of the S-protein of targeted virus - ACE2 interaction ( $\text{kcal mol}^{-1}$ ) into Coulomb (Left) and van der Waals (Right) averaged from 50 ns-long MD trajectories.

### 3. H-bond number and properties in the recognition of ACE2 to RBD

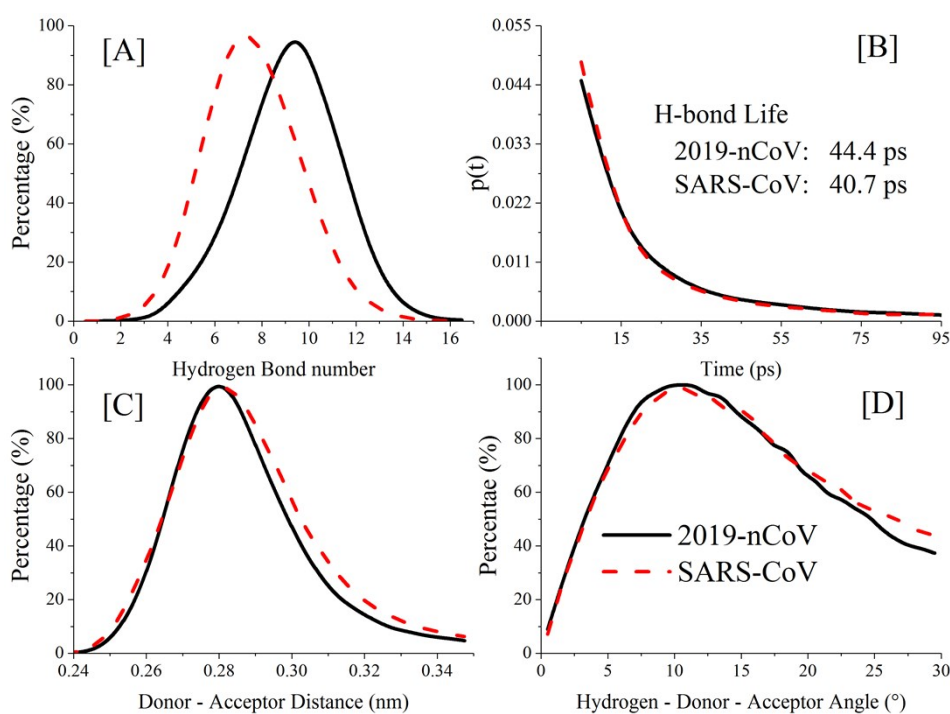


**Figure S2.** Intermolecular H-bond [A] number, [B] life, [C] distance, and [D] angle between ACE2 and S-protein of 2019-nCoV (black line) and SARS-CoV (red dotted line) sampled by 50,000 frames of 50-ns long time.

### 4. RMSD of ACE2 in unbound state

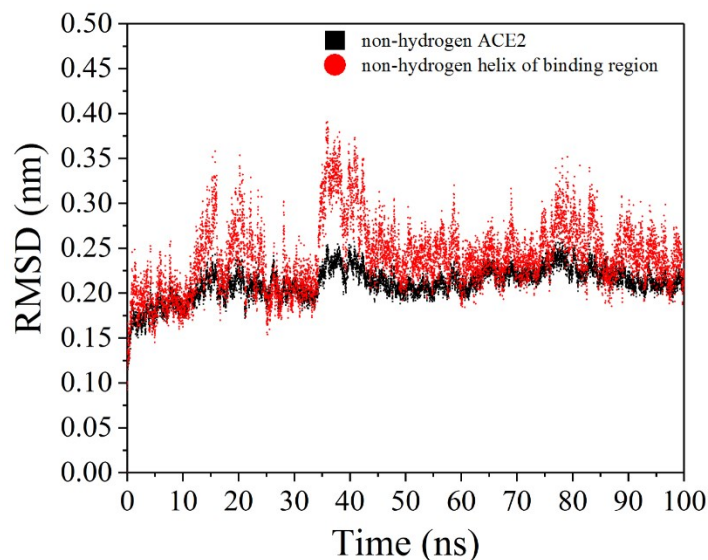


**Figure S3.** Time evolution of positional RMSD of the non-hydrogen atoms of ACE2 (black) and helix structure (red, residue 20 ~ 65 in crystal structure) in binding region in 100-ns single ACE2 solution plain simulation by superposing the non-hydrogen ACE2 atoms. The initial production run structures were chosen as the reference structure.

## 5. Residues superposing of unbound ACE2 to crystal structure

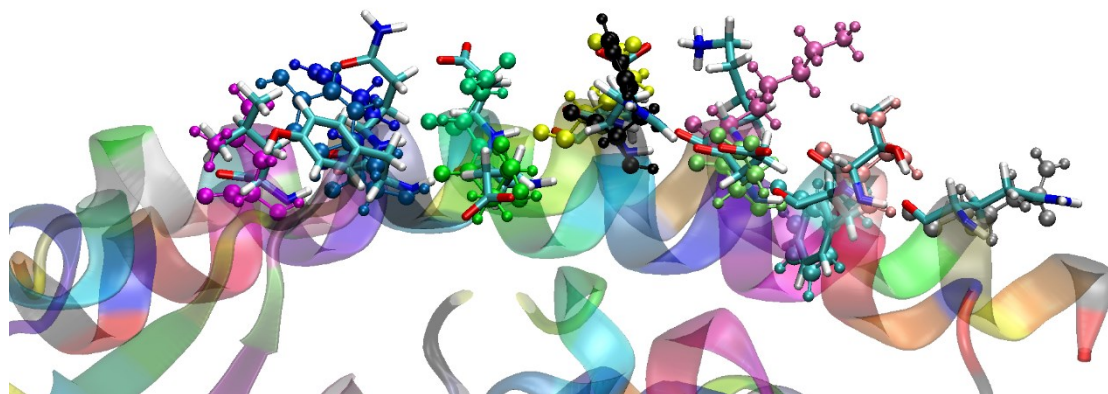


**Figure S4.** The snapshot of last frame of 100-ns long plain MD simulations of ACE2 superposed to crystal structure. The key residues in the binding region of ACE2 are represented by CPK (last MD configuration) and Licorice (crystal structure, PDB code: 6M0J), respectively.

## 6. RMSD of RBM of bound RBD

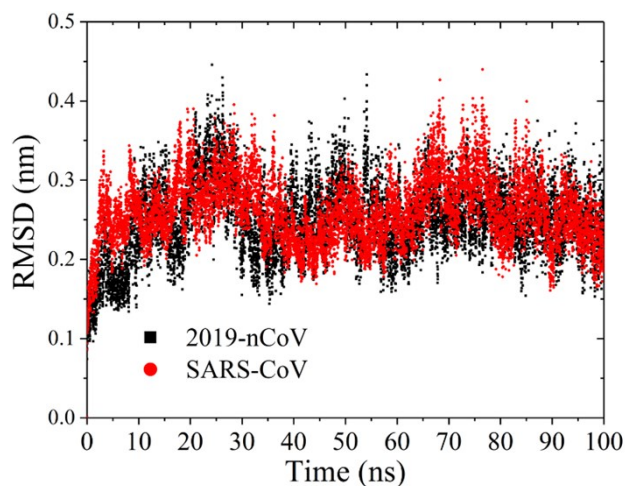


**Figure S5.** Time evolution of positional RMSD of the non-hydrogen atoms of the RBM of 2019-nCoV (black) and SARS-CoV (red) sampled by 100-ns long trajectories by superposing RBD core region. The initial production run structures were chosen as the reference structure.

## 7. RMSD of complexes of ACE2 with 2019-nCoV and SARS-CoV

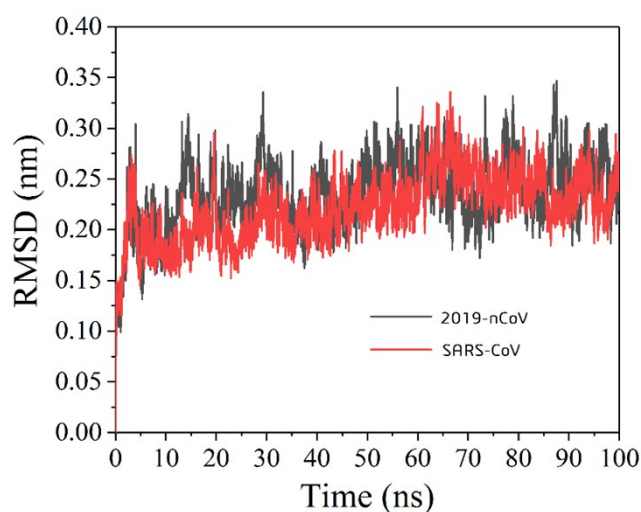


**Figure S6.** Time evolution of positional RMSD of the backbone atoms (CA, C, N) of the complex of ACE2 with 2019-nCoV (black) and SARS-CoV (red) sampled by 100-ns long trajectories by superposing these backbone atoms. The initial production run structures were chosen as the reference structure.

## 8. RMSD of single RBD in solution

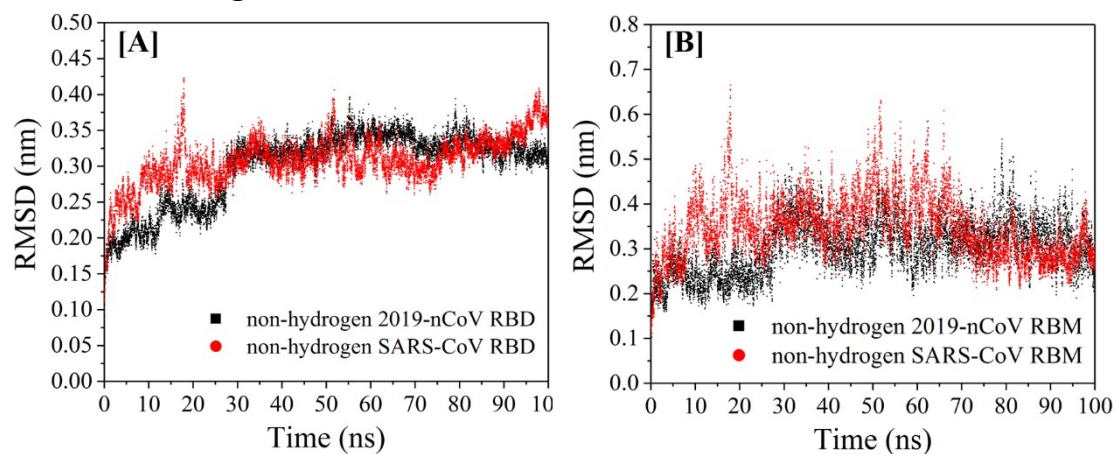


**Figure S7.** Time evolution of positional RMSD of the non-hydrogen atoms of [A] RBD (Left) of 2019-nCoV (black) and SARS-CoV (red) fitted by the non-hydrogen atoms of RBD, and [B] non-hydrogen atoms of RBM (Right) of 2019-nCoV (black) and SARS-CoV (red) fitted by the non-hydrogen atoms of RBD core region in their 100-ns single RBD solution plain simulation. The initial production run structures were chosen as the reference structure.

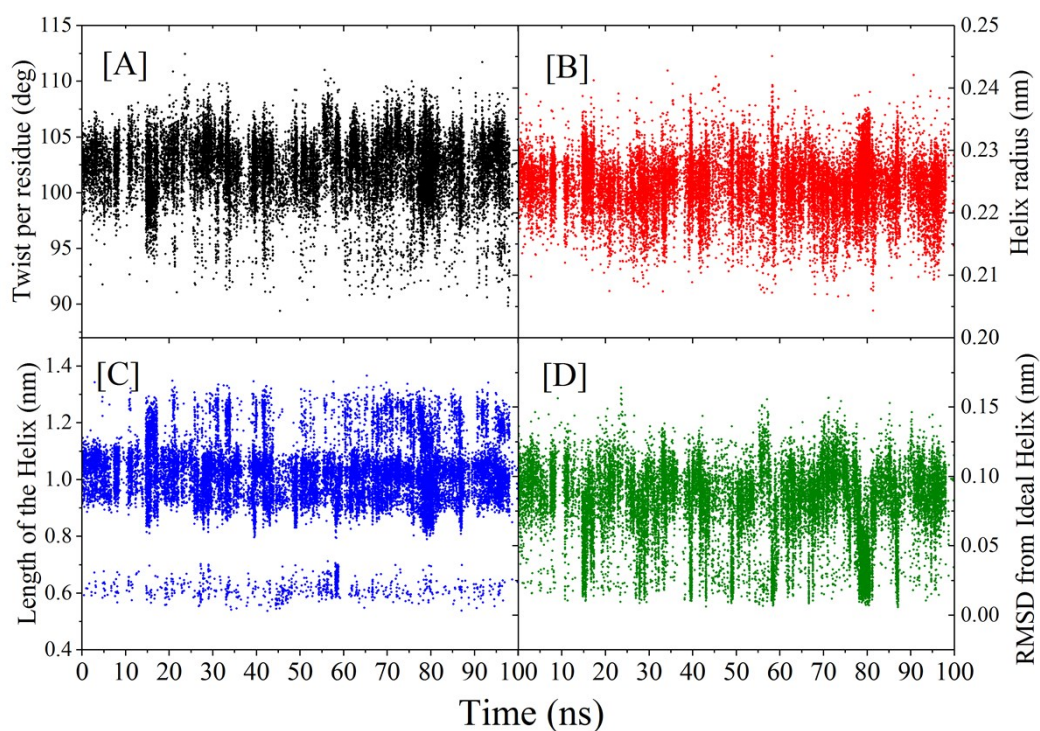
## 9. Relative free energy and interaction energy decomposition of annealed RBD

**Table S2.** The relative free energies ( $\Delta G$ , kcal/mol) and interaction energy components of RBD of 2019-nCoV and SARS-CoV with respect to their native conformation in bound state. The free energies were calculated by MM/GBSA method.

| Annealing<br>cycle | $\Delta G$ |       |              | energy decomposition |       |              |           |      |               |
|--------------------|------------|-------|--------------|----------------------|-------|--------------|-----------|------|---------------|
|                    | Gas        | sol   | Tot          | RBD-RBD              |       |              | RBD-Water |      |               |
|                    |            |       |              | Coul                 | vdW   | Tot          | Coul      | vdW  | Tot           |
| 2019-nCoV          |            |       |              |                      |       |              |           |      |               |
| 1                  | -165.5     | 115.4 | <b>-50.0</b> | -11.7                | -9.4  | <b>-21.0</b> | 23.0      | 5.6  | <b>28.6</b>   |
| 2                  | -188.0     | 134.2 | <b>-53.8</b> | -26.0                | 1.7   | <b>-24.3</b> | 56.2      | 5.0  | <b>61.2</b>   |
| 3                  | -275.7     | 193.0 | <b>-82.7</b> | -73.8                | 3.9   | <b>-69.9</b> | 161.6     | -7.5 | <b>154.2</b>  |
| 4                  | -196.6     | 146.0 | <b>-50.6</b> | -36.7                | -2.0  | <b>-38.7</b> | 126.9     | -2.3 | <b>124.6</b>  |
| 5                  | -270.0     | 196.8 | <b>-73.2</b> | -73.8                | 14.8  | <b>-59.0</b> | 154.5     | -6.6 | <b>147.9</b>  |
| 6                  | -103.2     | 68.8  | <b>-34.4</b> | 5.4                  | 23.6  | <b>29.0</b>  | -16.7     | -6.3 | <b>-23.0</b>  |
| 7                  | -196.6     | 137.6 | <b>-59.0</b> | -89.2                | 8.3   | <b>-80.9</b> | 127.0     | -4.7 | <b>122.3</b>  |
| 8                  | -199.1     | 123.2 | <b>-75.9</b> | -64.8                | -1.5  | <b>-66.3</b> | 144.3     | -4.8 | <b>139.5</b>  |
| 9                  | -148.6     | 105.1 | <b>-43.5</b> | -57.9                | 12.2  | <b>-45.7</b> | 43.7      | -8.9 | <b>34.8</b>   |
| 10                 | -225.6     | 166.7 | <b>-58.9</b> | -36.1                | 13.4  | <b>-22.7</b> | 91.1      | -4.9 | <b>86.2</b>   |
| SARS-CoV           |            |       |              |                      |       |              |           |      |               |
| 1                  | -62.7      | 15.4  | <b>-47.3</b> | 55.2                 | -5.1  | <b>50.1</b>  | -63.5     | 12.5 | <b>-51.0</b>  |
| 2                  | -126.6     | 74.6  | <b>-52.0</b> | 19.1                 | 3.9   | <b>22.9</b>  | -1.9      | -8.2 | <b>-10.1</b>  |
| 3                  | -30.8      | -25.2 | <b>-56.0</b> | 54.0                 | -9.0  | <b>45.0</b>  | -89.8     | 14.9 | <b>-74.9</b>  |
| 4                  | -128.3     | 61.4  | <b>-67.0</b> | 6.0                  | -1.3  | <b>4.7</b>   | 10.9      | -2.4 | <b>8.4</b>    |
| 5                  | 1.2        | -26.3 | <b>-25.1</b> | 56.2                 | 10.4  | <b>66.6</b>  | -131.4    | 2.9  | <b>-128.5</b> |
| 6                  | -105.3     | 51.9  | <b>-53.4</b> | 12.2                 | -1.6  | <b>10.6</b>  | -16.0     | -0.3 | <b>-16.4</b>  |
| 7                  | -76.4      | 26.9  | <b>-49.5</b> | 5.8                  | -0.5  | <b>5.3</b>   | 8.6       | 3.8  | <b>12.5</b>   |
| 8                  | -12.0      | -17.9 | <b>-29.9</b> | 60.4                 | 2.5   | <b>62.9</b>  | -141.5    | 8.8  | <b>-132.7</b> |
| 9                  | -62.1      | 23.7  | <b>-38.4</b> | 26.1                 | 15.8  | <b>41.9</b>  | -81.5     | -0.5 | <b>-82.1</b>  |
| 10                 | -136.1     | 79.2  | <b>-56.9</b> | -8.5                 | -12.1 | <b>-20.6</b> | 39.0      | 14.0 | <b>53.0</b>   |

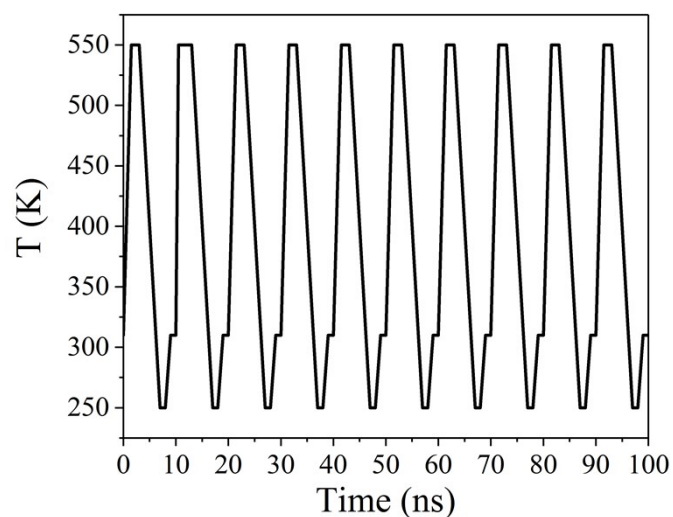


## 10. Time evolution of helical fragment in the annealed RBMD of 2019-nCoV



**Figure S8.** Time evolution of the helical fragment in the annealed RBMD of 2019-nCoV during the 100-ns long plain simulation. [A] average twist per residue, [B] helix radius, [C] helix length, [D] positional backbone RMSD with respect to ideal helix structure.

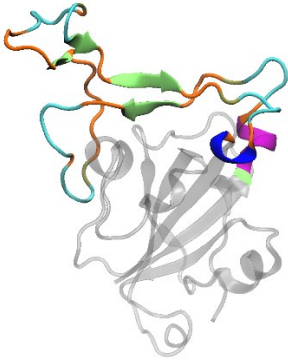
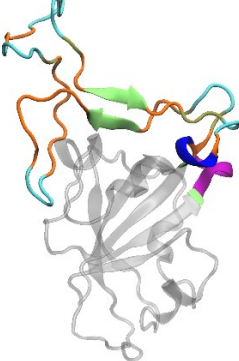
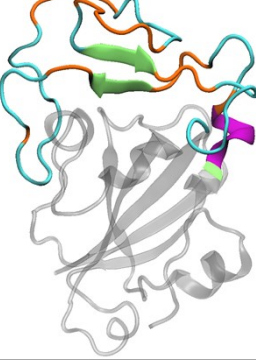
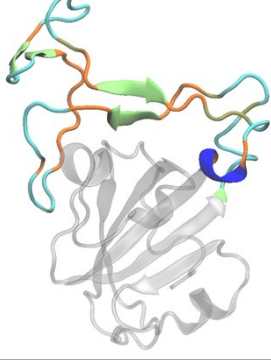
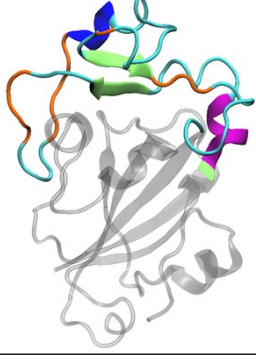
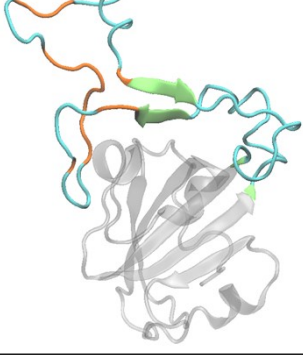
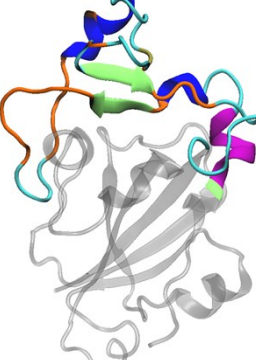
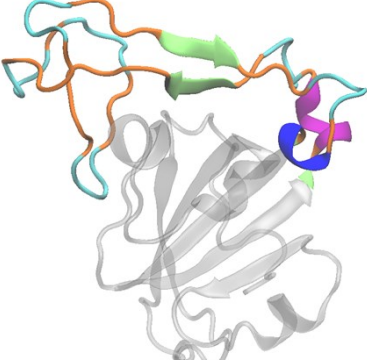
## 11. Temperature control scheme in simulated annealing

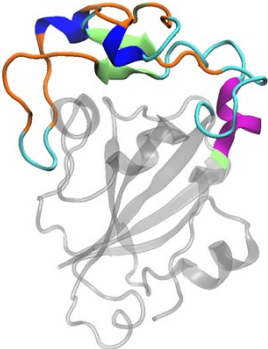
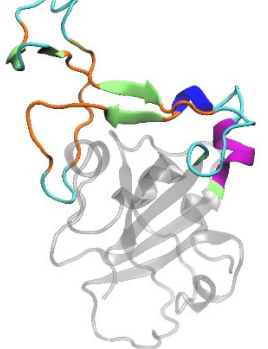
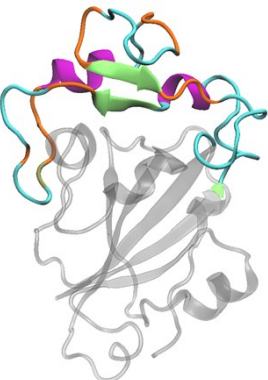
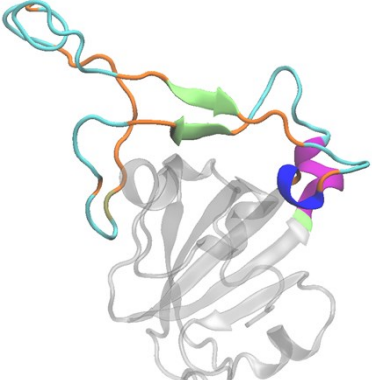
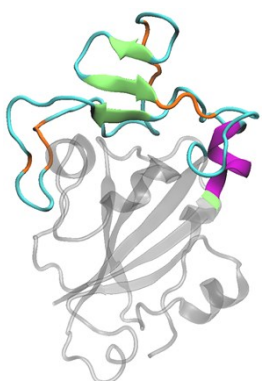
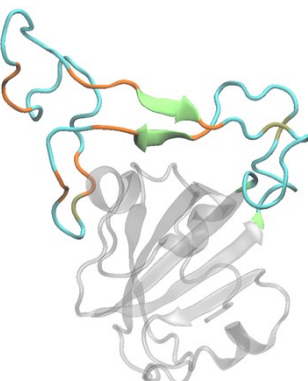
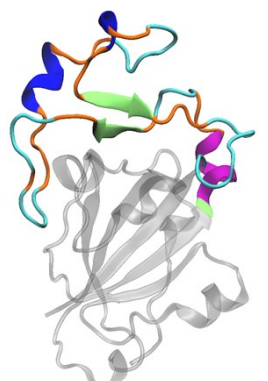
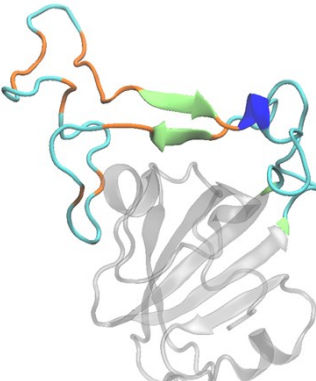


**Figure S9.** Temperature control scheme in simulated annealing in 100-ns long simulations for 10 cycles.

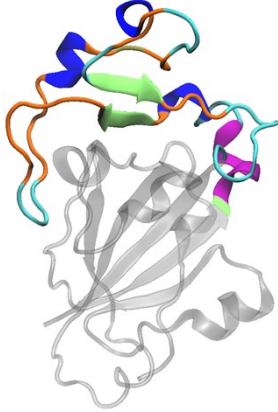
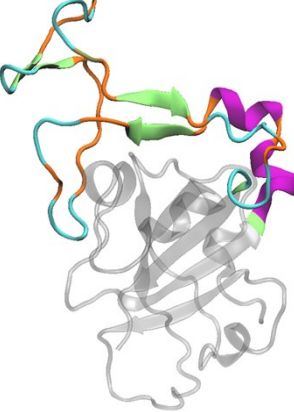
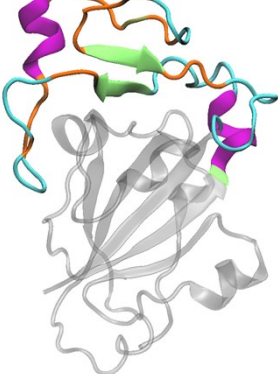
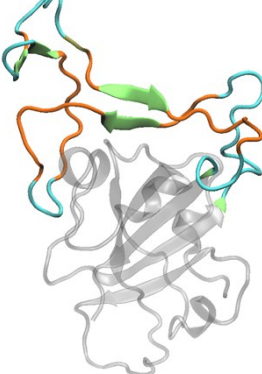
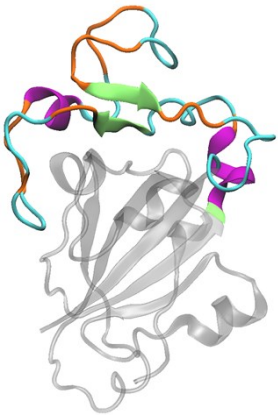
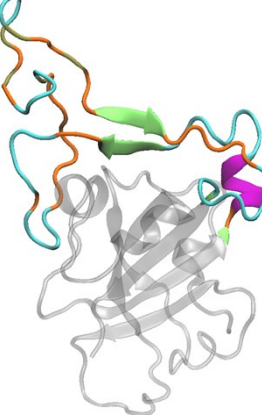
## 12. Annealed structures for RBD of 2019-nCoV and SARS-CoV

**Table S3.** The comparison of bound and annealed configuration of each cycle of RBD of 2019-nCoV (Left) and SARS-CoV (Right) in 10 cycles.

| cycle | 2019-nCoV   | SARS-CoV   |
|-------|---|--|
| bound |    |    |
| 1     |   |   |
| 2     |  |  |
| 3     |  |  |

|   |   |  |
|---|---|--|
| 4 |    |    |
| 5 |    |    |
| 6 |   |   |
| 7 |  |  |



|    |   |  |
|----|---|--|
| 8  |    |    |
| 9  |   |   |
| 10 |  |  |

### 13. H-bond distribution difference for bound and annealed RBD

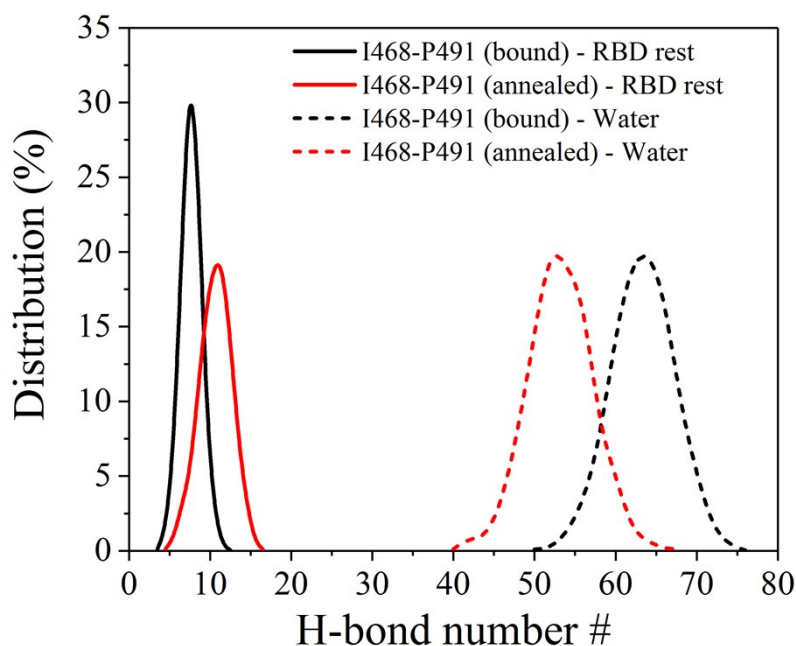


**Figure S10.** The H-bond number distribution between I468-P491 of 2019-nCoV and RBD rest (solid line), and between I468-P491 of 2019-nCoV and water (dotted line). The I468-P491 is in native shape in bound configuration (black), while folded shape in annealed configuration (red).

### 14. Diffusion coefficient of bound and annealed RBD

**Table S4.** The diffusion coefficient  $D$  ( $10^{-6}\text{cm}^2/\text{s}$ ) of bound and annealed RBD of 2019-nCoV and SARS-CoV calculated by fitting 0~20 ns time evolution of MSD (Figure S11) from 100 ns plain MD trajectories in water at 310 K. The correlation coefficients  $R^2$  for fitting MSD and time linear equations were also shown. The standard deviation of  $D$  was calculated by Figure S11 (15 ~ 20 ns).

|                                       | 2019-nCoV |          | SARS-CoV |          |
|---------------------------------------|-----------|----------|----------|----------|
|                                       | bound     | annealed | bound    | annealed |
| $D$ ( $10^{-6}\text{cm}^2/\text{s}$ ) | 2.51      | 3.60     | 2.67     | 2.93     |
| SD ( $10^{-6}\text{cm}^2/\text{s}$ )  | 0.21      | 0.11     | 0.13     | 0.13     |
| $R^2$                                 | 0.980     | 0.999    | 0.995    | 0.999    |

## 15. Time evolution of MSD for RBD

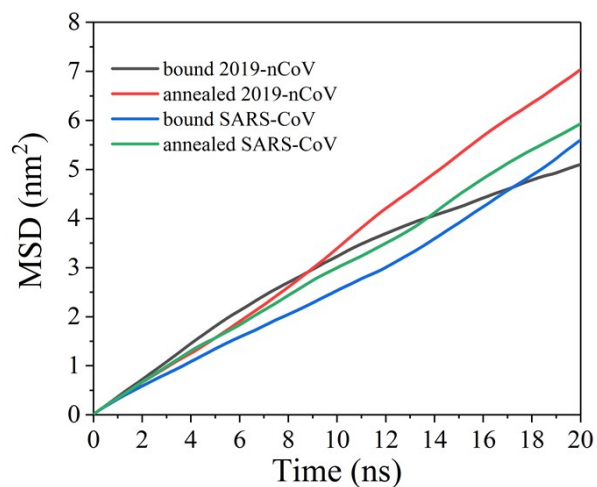


**Figure S11.** MSD as a function of time for the non-hydrogen atoms of bound and annealed RBD of 2019-nCoV and SARS-CoV, respectively.

## 16. Energy decomposition of bound and annealed configurations

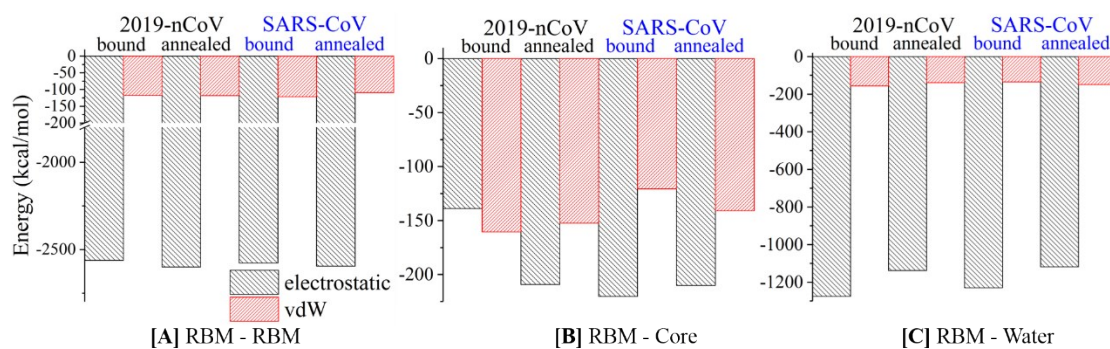


**Figure S12.** The energy decomposition of RBM with [A] itself, [B] Core, and [C] water, respectively, into electrostatic (black) and vdW (red).

## 17. Time evolution of H-bond number in the recognition of ACE2 to RBD

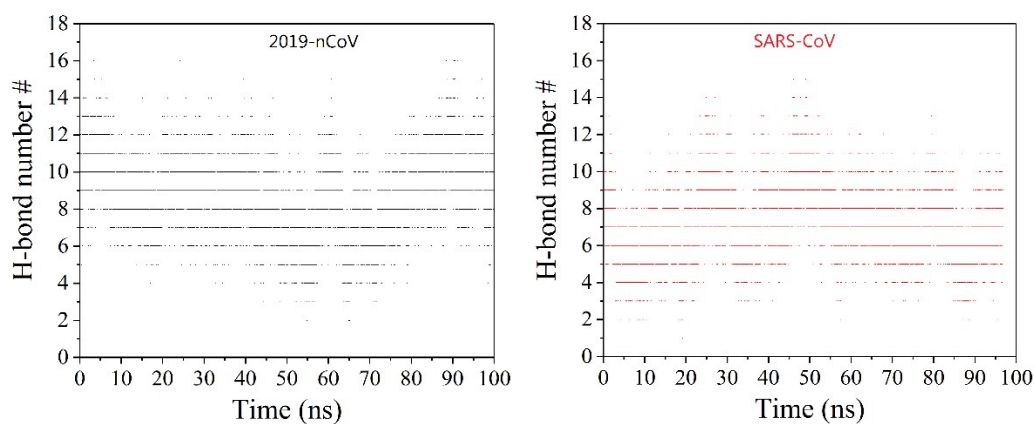


**Figure S13.** Time evolution of H-bond number between ACE2 and 2019-nCoV (left), SARS-CoV (right) during 100 ns plain MD simulations.

## 18. Note on the MM/GBSA results in Figure 1?

The MM/GBSA method is an approximate algorithm in calculating binding affinities. In recent years of review<sup>1, 2</sup> and benchmark<sup>3-7</sup> work, MM/GBSA has been reported good fitness in binding affinities for ligand-protein interaction, especially qualitatively, with low computational cost. This method is also expected to be applied to the evaluation of protein-protein interactions (PPIs), which is quite important for understanding the biological processes but difficult for calculation. In recent years, a series of benchmark results<sup>8-10</sup> involving the evaluation of PPIs based on MM/GBSA have been reported, and they this method exhibited good performance in reproducing and predicting binding affinities of PPIs based on plain MD simulations, and proposed that it could be used as an effective method for preliminary screening. The calculation of entropy may result in opposite consequences: sometimes it may improve the calculated binding free energy with better agreement with the experimental result, and sometimes cause larger deviation away from the experimental data.<sup>11, 12</sup> It is usually an effective way to offset the contribution of entropy in similar binding systems to achieve qualitative results of PPIs.<sup>12</sup> Benefited from their stability in their conformation prior to and after binding to each other, here the MM/GBSA method was used to obtain a qualitative understanding of the binding of the RBM of the spike protein and the ACE2 rather than very accurate calculation on the binding strength considering the quality of the method.

## 19. Binding free energies of ACE2 with RBD

**Table S5.** Binding free energies (kcal/mol) and their standard deviations (SD), standard errors of the mean (SEM) of ACE2 with 2019-nCoV and SARS-CoV calculated by MM/GBSA method.

| frames | 2019-nCoV                |     |     | SARS-CoV                 |     |     |
|--------|--------------------------|-----|-----|--------------------------|-----|-----|
|        | $\Delta G_{\text{bind}}$ | SD  | SEM | $\Delta G_{\text{bind}}$ | SD  | SEM |
| 50     | -49.9                    | 4.5 | 0.6 | -22.6                    | 4.1 | 0.6 |
| 100    | -50.3                    | 4.6 | 0.5 | -24.1                    | 4.5 | 0.5 |
| 150    | -50.0                    | 4.9 | 0.4 | -23.8                    | 4.3 | 0.4 |
| 200    | -51.6                    | 5.5 | 0.5 | -23.7                    | 4.4 | 0.3 |
| 500    | -53.2                    | 5.8 | 0.3 | -25.1                    | 4.6 | 0.2 |
| 1000   | -50.8                    | 6.3 | 0.2 | -27.0                    | 5.3 | 0.2 |
| 2000   | -48.1                    | 6.4 | 0.1 | -27.9                    | 5.4 | 0.1 |
| 5000   | -48.9                    | 6.7 | 0.1 | -27.7                    | 5.2 | 0.1 |
| 10000  | -49.4                    | 6.6 | 0.1 | -27.3                    | 5.3 | 0.1 |

## 20. Quantitative analysis of IGM analysis

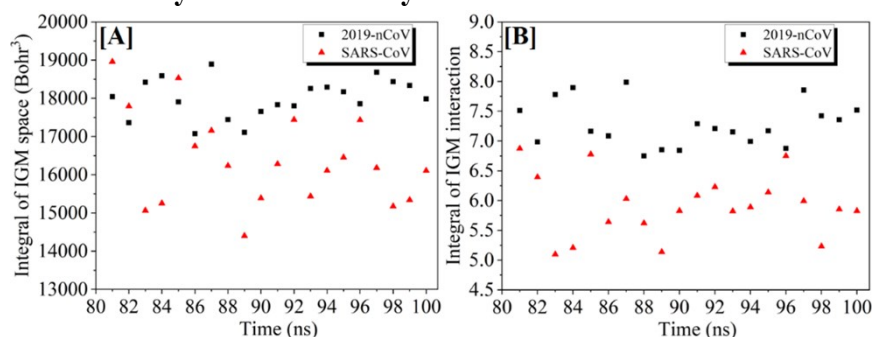


**Figure S14.** The integral of [A] interaction space and [B] interaction strength of ACE2 with RBD of 2019-nCoV (black square) and SARS-CoV (red triangle) by IGM analysis with the time evolution of 80-100 ns simulations.

## 21. Cluster analysis

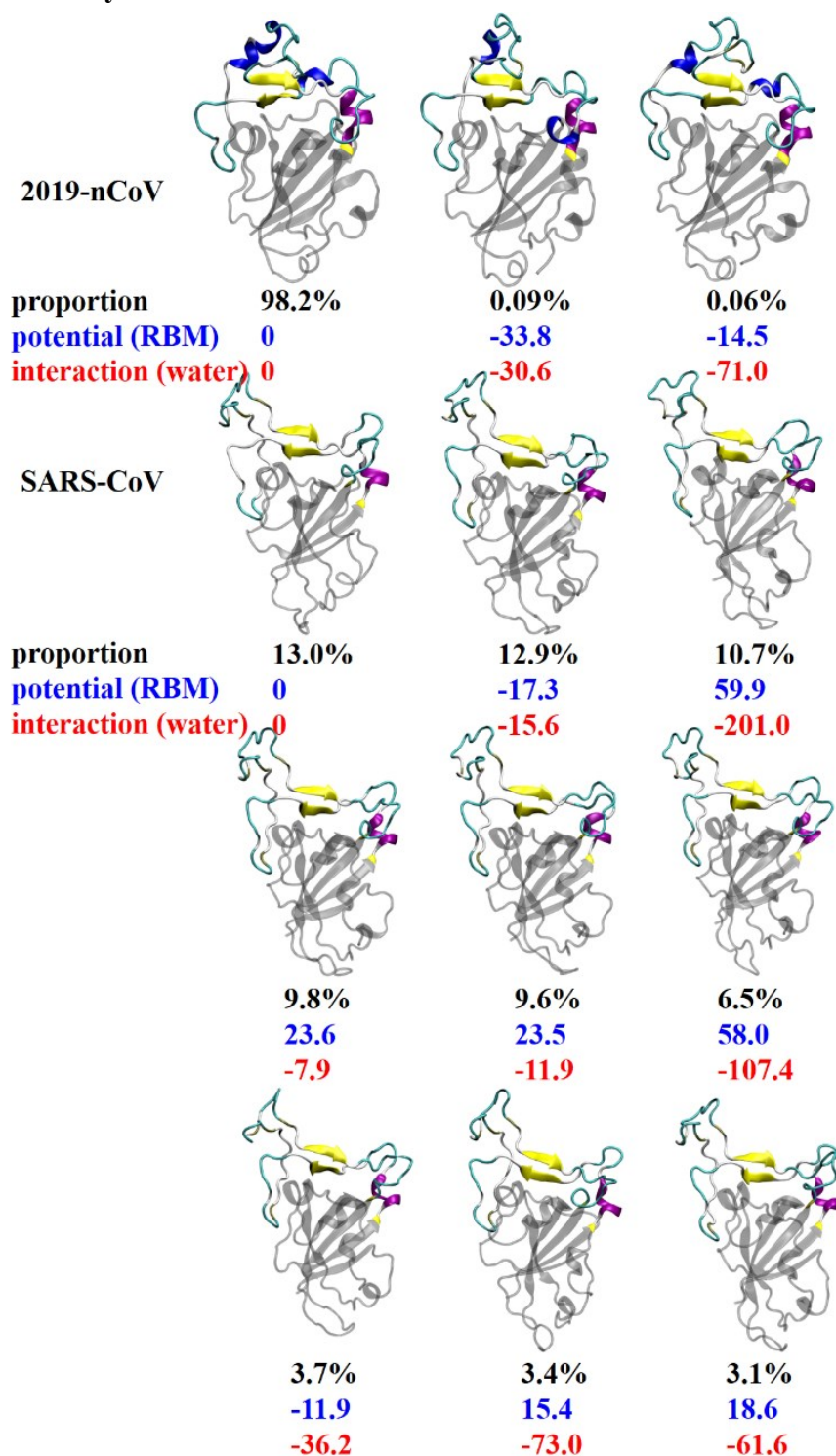


**Figure S15.** The central structures of the top clusters in the 100-ns simulations after simulated annealing of RBM backbone of 2019-nCoV (top) and SARS (bottom). Each cluster's proportion (black), average relative potential energy of RBM to largest cluster (blue), and average relative interaction energy between RBM and water to largest clusters (red) were also presented (kcal/mol).



## References:

1. S. Genheden and U. Ryde, Expert opinion on drug discovery, 2015, 10, 449-461.
2. E. Wang, H. Sun, J. Wang, Z. Wang, H. Liu, J. Z. H. Zhang and T. Hou, Chemical reviews, 2019, 119, 9478-9508.
3. T. Hou, J. Wang, Y. Li and W. Wang, Journal of chemical information and modeling, 2011, 51, 69-82.
4. H. Sun, Y. Li, S. Tian, L. Xu and T. Hou, Physical Chemistry Chemical Physics, 2014, 16, 16719-16729.
5. F. Adasme-Carreño, C. Muñoz-Gutierrez, J. Caballero and J. H. Alzate-Morales, Physical Chemistry Chemical Physics, 2014, 16, 14047-14058.
6. S. S. Çınaroğlu and E. Timuçin, Briefings in Bioinformatics, 2019.
7. S. K. Mishra and J. Koča, The Journal of Physical Chemistry B, 2018, 122, 8113-8121.
8. F. Chen, H. Liu, H. Sun, P. Pan, Y. Li, D. Li and T. Hou, Physical Chemistry Chemical Physics, 2016, 18, 22129-22139.
9. G. Weng, E. Wang, F. Chen, H. Sun, Z. Wang and T. Hou, Physical Chemistry Chemical Physics, 2019, 21, 10135-10145.
10. E. Wang, G. Weng, H. Sun, H. Du, F. Zhu, F. Chen, Z. Wang and T. Hou, Physical Chemistry Chemical Physics, 2019, 21, 18958-18969.
11. H. Sun, L. Duan, F. Chen, H. Liu, Z. Wang, P. Pan, F. Zhu, J. Z. H. Zhang and T. Hou, Physical Chemistry Chemical Physics, 2018, 20, 14450-14460.
12. T. Hou and R. Yu, Journal of medicinal chemistry, 2007, 50, 1177-1188.